Environmental Science & Technology

pubs.acs.org/est Article

Cooling Effects on Capillary Sealing in CO_2−Plume Geothermal Systems: Capillary Pressure Modeling and Leakage Assessment

Chaojie Di, Fei Tian,* Liang Zhao,* Peng Deng, Haoming Ma, Benjieming Liu, Long Peng, and Zhangxin Chen*

Cite This: *Environ. Sci. Technol.* 2026, 60, 6149−6161

ABSTRACT: The CO_2−Plume Geothermal (CPG) technology is an emerging approach that utilizes CO_2 as a working fluid to simultaneously extract geothermal energy and achieve long-term underground carbon sequestration. The circulation of cold CO_2 significantly lowers reservoir temperature and alters rock wettability, which threatens the long-term security of CO_2 sequestration by weakening the capillary sealing capacity of caprock. To address this concern, we investigate the mechanisms by which cooling-induced wettability alteration affects the capillary sealing capacity of CPG caprock and quantitatively evaluate the associated leakage risks. First, we propose a temperature-saturation dependent capillary pressure (TSPC) model to quantify the impact of temperature variations on caprock capillary sealing capacity. Subsequently, the TSPC model is integrated into our in-house numerical reservoir simulator to quantitatively assess CO_2 leakage for a field-scale CPG operation. Simulation results show that temperature reduction during CPG operation decreases capillary pressure by 45%−87%, which substantially undermines the ability of the caprock to prevent CO_2 upward breakthrough. The decline in capillary pressure weakens the sealing capacity and leads to nearly 50,000 tons of CO_2 leakage in a representative CPG reservoir simulation. The above results demonstrate a previously unrecognized CO_2 leakage mechanism in CPG systems caused by cooling-induced wettability alteration. In addition, we propose practical mitigation strategies to address this leakage risk and enhance the long-term security of CO_2 sequestration after CPG operations.

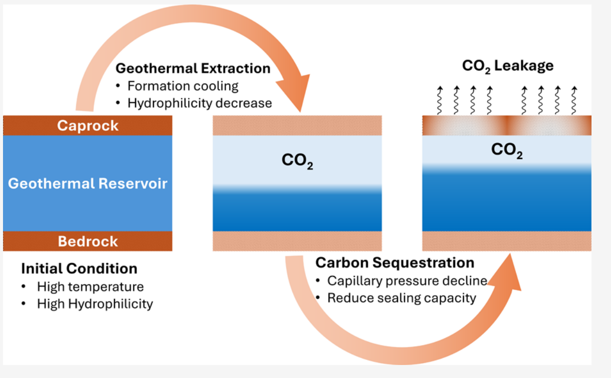

KEYWORDS: *CCUS, CO_2-plume geothermal system, geological carbon storage, rock wettability, numerical reservoir simulation*

1. INTRODUCTION

The increasing concentrations of greenhouse gases in the atmosphere pose a significant threat to the global climate, highlighting the urgent need to transition from conventional fossil fuels to green and renewable energy resources.[1−4] A CO_2−Plume Geothermal (CPG) system represents a cutting-edge integration of geothermal energy extraction with carbon capture, utilization, and storage (CCUS).[5−7] By using CO_2 as a working fluid, CPG systems address two critical global challenges: mitigating global warming and increasing energy sustainability.[8] In a CPG system, CO_2 is injected into deep hot aquifers to absorb heat, and then it is produced to the surface for energy generation. After extraction, the cooled CO_2 is either recycled or permanently stored in target geological formations. Higher mobility in porous media and better heat transfer efficiency on surface generators make CO_2 particularly effective for extracting geothermal energy from deep hot aquifers.[9] Moreover, CPG systems provide an efficient approach to permanently storing CO_2 in subsurface formations and reducing the negative environmental impact of energy production.[10] This dual functionality not only enhances the economic viability of CCUS projects but also supports the transition toward renewable and sustainable energy systems.

The development of CPG systems has drawn increasing attention in recent years, particularly regarding the challenges associated with CO_2 leakage.[11−13] Leakage pathways include caprock fractures, fault zones, and poorly sealed wells, presenting unique challenges and were highlighted by prior studies.[14−19] Rock fractures, often formed by stress or reservoir pressure changes, have been identified as critical pathways for CO_2 leakage.[14,15] Fault zones, due to their complex geological structure, can act as conduits or barriers for CO_2 migration, depending on their sealing capacity.[17,18] Poorly sealed wells, particularly abandoned or improperly completed wells, pose significant risks due to potential cement degradation and

Received: June 22, 2025
Revised: January 23, 2026
Accepted: January 23, 2026
Published: January 29, 2026

casing failures, as observed in field studies of CO_2 storage projects.[19,20] Both rock and cement are porous media with nonzero permeability, which means that only reducing permeability to prevent CO_2 leakage is impractical for long-term sequestration projects. Extensive studies have demonstrated that utilizing effective sealing mechanisms is critical for preventing CO_2 migration into overlying formations, thereby ensuring storage security in the post-CPG period.[21] Among the various factors influencing leakage, capillary pressure plays a critical role. Experiments and numerical simulations have demonstrated that higher capillary pressure in caprock formations can significantly reduce the risk of CO_2 leakage.[22,23] Temperature reduction in the formation during geothermal extraction can alter the gas−water contact angle and interfacial tension in its caprock, thereby weakening its capillary sealing capacity.[24−27] Despite the importance of this phenomenon for assessing CO_2 storage capacity and long-term security, its influences have not been adequately investigated in the existing literature. Although some experimental studies have qualitatively demonstrated the effects of temperature on rock wettability,[24,26,27] their implications for field-scale CPG systems are not explored. Filling these research gaps is essential for optimizing CPG design and operation while ensuring long-term CO_2 containment.

Capillary pressure prediction is essential for assessing cooling-induced CO_2 leakage risks from the numerical simulations of CPG systems.[22] Pore-scale modeling provides a more detailed approach by simulating fluid flow within individual rock pores.[28,29] This method allows for a deeper understanding of how pore geometry, wettability alteration, and fluid properties influence capillary pressure. Advances in imaging technologies, such as X-ray microtomography, have enabled the construction of high-resolution pore-scale models.[30,31] Although these models are invaluable for studying microscopic interactions, they are computationally intensive and therefore not suitable for large-scale reservoir simulations. Recent developments in artificial intelligence (AI) have introduced data-driven methods for predicting capillary pressure.[32,33] AI models offer a way to incorporate nonlinear dependencies and reduce reliance on predefined functional forms. However, their success depends heavily on the availability and quality of training data. Empirical models are the most widely used methods for predicting capillary pressure in numerical CPG reservoir simulations.[34,35] Based on experimental data, these models, such as the Brooks-Corey and van Genuchten models, describe a capillary pressure-saturation relationship using simplified equations.[36,37] While these models are computationally efficient and adaptable to different rock types, they often fail to capture the wettability alteration under varied formation temperatures, limiting their applicability to CPG systems. Some recent studies utilized microscopic experimental data, gas−water contact angles and interfacial tension (IFT), to predict capillary pressure under varying formation pressures.[22,38] Nevertheless, they are not applicable to CPG systems, as temperature variations play a dominant role during geothermal extraction, while pressure changes are minimal. To our knowledge, a capillary pressure model that considers the effects of temperature variation remains an unaddressed gap in large-scale CPG reservoir simulations.

The primary objective of this study is to evaluate how temperature reduction alters the capillary pressure in caprocks and its potential effect on the sealing capacity of caprocks. This is achieved by developing a temperature-saturation dependent capillary pressure (TSPC) model. It integrates microscopic experimental data, contact angles and IFTs to quantify the thermal effect on capillary pressure. The developed model is incorporated into our numerical CPG simulator[39] to assess the impact of cooling on caprock sealing integrity through field-scale CO_2 simulations of CO_2 underground migration and breakthrough behavior. The simulation results uncover a CO_2 leakage mechanism in CPG systems caused by cooling-induced wettability alteration, which has been largely overlooked in previous CPG research. The remainder of this paper is organized as follows: Section 2 introduces the methodologies, including the mathematical model for numerical CPG simulation, the development of the TSPC model, and the setup of simulation cases; Section 3 presents the modeling and field-scale simulation results; Section 4, which discusses the broader implications of the findings for CO_2 storage security in CPG systems.

2. METHODOLOGIES

2.1. Mathematical Model for Numerical CPG Simulation

The mathematical framework for geothermal reservoir simulation in this study is built on the principles of multiphase fluid flow within porous media, underground heat transfer, matter and energy conservation. Multiphase fluid flow in porous media is governed by Darcy's Law, an empirical formula that calculates the flow velocity ($\boldsymbol{v}$) through a porous medium based on its permeability and potential differences, including phase pressure and gravity. It is expressed as

$$\boldsymbol{v}_\alpha = -\boldsymbol{k}(\nabla P_\alpha - \Upsilon_\alpha \nabla h)\left(\frac{k_r}{\mu}\right)_\alpha, \; \alpha = g, w \tag{1}$$

where $\boldsymbol{k}$ is the absolute permeability of the rock; P refers to the phase pressure; Υ represents phase gravity; h is block depth; k_r indicates phase relative permeability; μ denotes phase viscosity; g, w means CO_2-rich phase and aqueous phase, respectively. Because the fluid velocity in the formation is very low, the fluid and rock are assumed to share the same temperature within each grid block. Under this condition, heat transfer along with fluid flow and heat conduction due to temperature difference dominate heat flow within the reservoir. Heat conduction is modeled using Fourier's Law, which describes the heat transfer due to temperature gradients:

$$\boldsymbol{Q}_{cd} = \boldsymbol{\lambda} \nabla T \tag{2}$$

where $\boldsymbol{Q}_{cd}$ is heat flux due to conduction; $\boldsymbol{\lambda}$ represents the thermal conductivity of fluid or rock; ∇T refers to the temperature gradient between two adjacent grids; The heat transfer along with fluid flow within the subsurface geothermal formation is described by the following equation:

$$\boldsymbol{Q}_{cv} = \rho \boldsymbol{v} E_h(P, T) \tag{3}$$

where $\boldsymbol{Q}_{cv}$ is heat flux due to fluid flow; ρ refers to molar density; $\boldsymbol{v}$ indicates flow velocity calculated from eq 1; E_h represents the specific enthalpy of fluid. The mass conservation equation for two-phase flow (CO_2-rich phase and aqueous phase) can be derived by combining the principle of conservation of mass with Darcy's Law. The governing equation for each component (CO_2 and H_2O) is given by

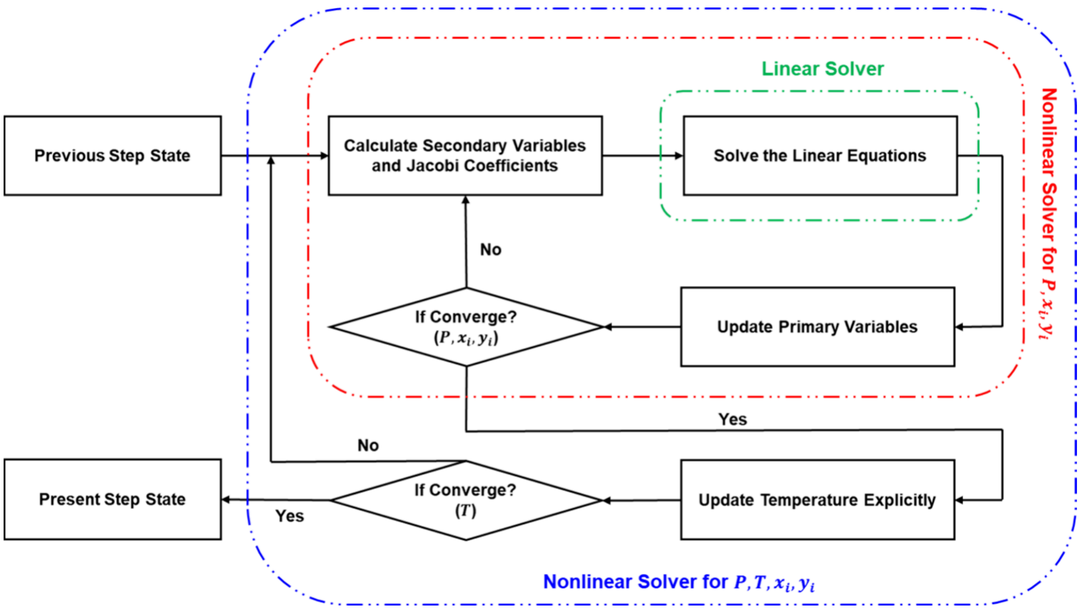

Figure 1. Fully implicit sequential solution workflow for geothermal reservoir simulation.

$$\frac{\partial(\varphi[x_i\rho_w S_w + y_i\rho_g S_g])}{\partial t} + \nabla\cdot(x_i\rho_w \boldsymbol{v}_w + y_i\rho_g \boldsymbol{v}_g) = q_i,\ i = CO_2,\ H_2O \tag{4}$$

ϕ denotes rock porosity; x_i and y_i are the mole fraction of i-th component in the aqueous phase and CO_2-rich phase, respectively; S refers to phase saturation; t is time; q_i represents the molar well flux of i-th component. Combining the above heat flux components with mass conservation and accounting for heat source or sink terms from well flux. It gives the heat conservation equation:

$$\sum\nolimits_{\alpha=g,w,s}\left[\frac{\partial}{\partial t}(\rho_\alpha \phi S_\alpha E_{h,\alpha}) + \nabla\cdot(\mathbf{Q}_{cv} - \phi S_\alpha \mathbf{Q}_{cd})\right] = Q_w \tag{5}$$

In this equation, we denote the solid phase (rock) by $\alpha = s$. As convention, set the "saturation" of the solid phase as $S_s = \frac{(1-\phi)}{\phi}$ and its "Darcy flux" is equal to zero. Q_w is the well heat flux. The fluid properties, including density, viscosity, specific enthalpy and composition (x_i and y_i), are predicted using pregenerated two-dimensional (temperature and pressure) property tables. The composition tables are obtained by performing phase equilibrium calculations using the Peng–Robinson equation of state with the Søreide and Whitson modification (PR-SW EOS).[40,41] Pure CO_2 and water phase density and viscosity data are retrieved from the NIST Chemistry WebBook.[42] The specific enthalpy tables for each component are also obtained from the NIST Chemistry WebBook, and the specific phase enthalpies are calculated by ideal mixing based on the specific enthalpies of components. Detailed solubility and fluid properties data for CO_2/water can be found in Appendix C.

Figure 1 illustrates the solution methodology for the mathematical model governing geothermal reservoir simulation at each time step. This approach provides a fully implicit solution of all variables, including temperature, pressure, and mole fractions, across all grid blocks. Initially, pressure and mole fractions are solved simultaneously using the Newton–Raphson method, which efficiently handles the coupled nonlinear equations. Subsequently, temperature is calculated using an explicit method to provide an initial estimate. Finally, the temperature is updated using an iterative implicit method to obtain an accurate solution, ensuring consistency across the energy conservation equation. This workflow balances numerical stability with computational efficiency, enabling robust simulation of geothermal reservoir dynamics.

2.2. Temperature-Saturation Dependent Capillary Pressure (TSPC) Model

Capillary pressure is the pressure difference across the interface of two immiscible fluids, driven by capillary forces. In existing commercial software,[43−45] for a CO_2-brine two-phase system, P_c depends solely on gas saturation. The pressure of the CO_2-rich phase can be calculated from the aqueous phase pressure using the equation:[46]

$$P_g = P_w + P_c(S_g) \tag{6}$$

Due to its lower density compared to water, the supercritical CO_2-rich phase naturally rises to the top of the aquifer driven by buoyant forces. The upward movement facilitates the recovery of supercritical CO_2 at the top of the formation but also poses a risk of leakage if the sealing capacity of the caprock is insufficient. According to eq 6, capillary pressure can prevent the upward migration of the CO_2-rich phase caused by its lower density. Thus, the P_c plays a pivotal role in carbon sequestration after a CO_2-plume geothermal extraction due to its ability to prevent CO_2 leaks from seal formation. eq 6 is applicable when capillary pressure is assumed to be independent of formation temperature and pressure, although this assumption may lead to significant errors in capillary pressure prediction during the CPG operation. Numerous experimental studies have shown that capillary pressure is significantly influenced by temperature and pressure, making it impractical to rely only on gas saturation for its estimation. In this study, we developed a temperature-saturation dependent capillary pressure model, extending the previous equations to

https://doi.org/10.1021/acs.est.5c08417
Environ. Sci. Technol. 2026, 60, 6149−6161

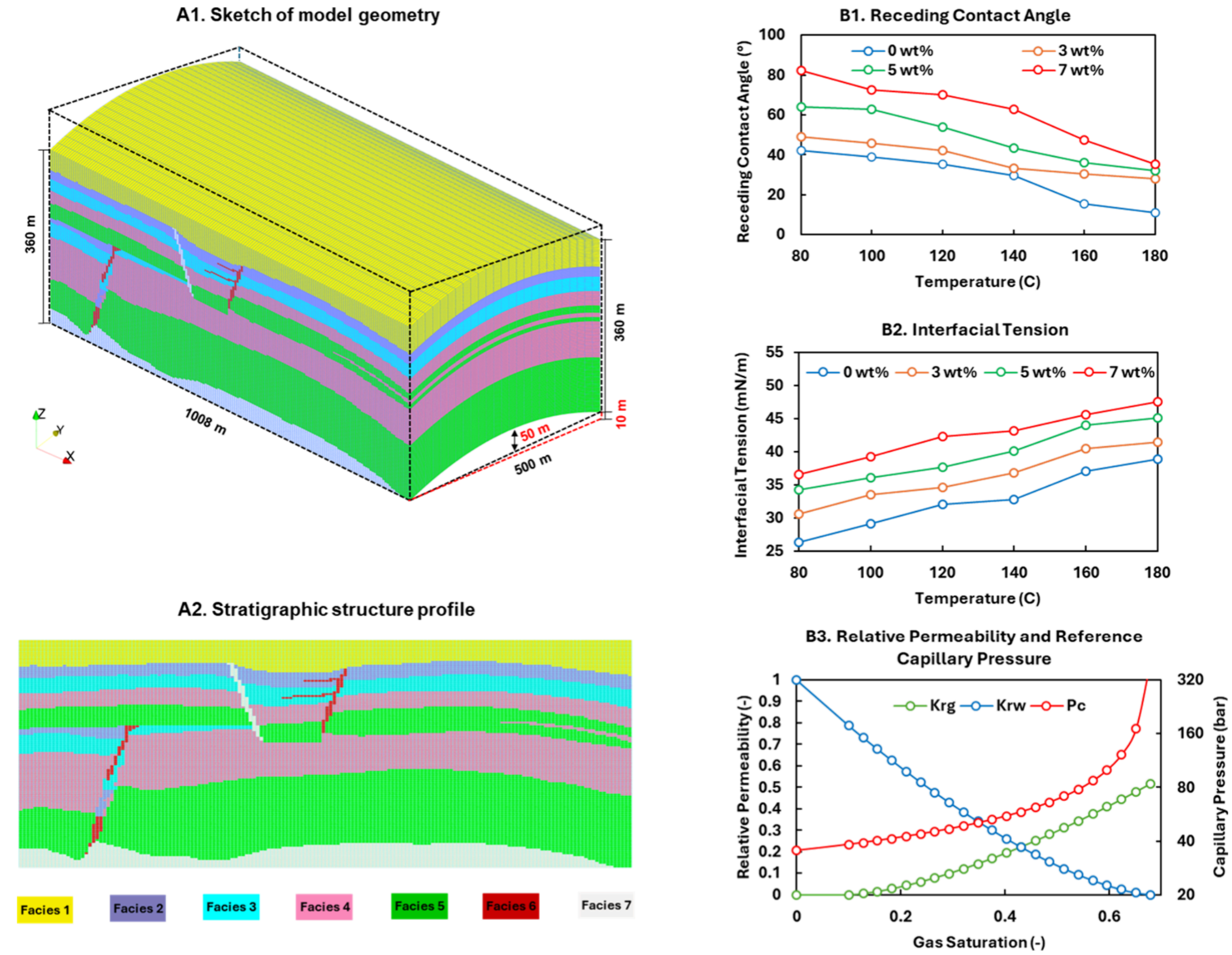

Figure 2. Numerical geological model and caprock wettability data set for CPG simulation.

better capture the impact of temperature variations on capillary pressure. To establish this model, several simplifying assumptions were made. First, the rock and fluid phases within each grid block are assumed to be at the same temperature and saturation, given the relatively low fluid velocity in geological formations. Second, the variation of capillary pressure with temperature is primarily attributed to temperature-dependent changes in interfacial tension and contact angle, which reflect the effect of wettability alteration. Third, temperature-induced mineral reactions, rock−fluid chemical alterations, and thermally driven changes in pore geometry are neglected within the simulated temperature range, so the pore-size distribution parameters are considered constant. Based on these assumptions, the capillary pressure can be determined using the Young−Laplace equation, as follows:

$$P_c(T,\ S_g) = \frac{2\sigma(T)\cos[\theta(T)]}{R(S_g)} \tag{7}$$

where θ denotes the contact angle between the aqueous and CO_2-rich phases; σ represents the interfacial tension (IFT) between these two phases; R is the radius of the largest pore throat that is saturated by the aqueous phase at a specific gas saturation. A reference capillary pressure−saturation $[P_c^{ref}(S_g)]$ curve at a selected reference temperature can be obtained from experimental measurements. The capillary pressure at different temperatures is obtained by scaling the reference curve using the Young−Laplace equation. Finally, the temperature-saturation dependent capillary pressure model is expressed as follows:

$$P_c(T,\ S_g) = f_s(T)P_c^{ref}(S_g) \tag{8}$$

In this equation, f_s denotes the scaling factors; P_c^{ref} represents the reference capillary pressure. The scaling factor f_s is derived from the Young−Laplace equation and is defined as

$$f_s = \frac{\sigma(T)\cos[\theta(T)]}{\sigma^{ref}\cos[\theta^{ref}]} \tag{9}$$

where σ^{ref} and θ^{ref} are IFT and contact angle at the reference temperature. This model integrates experimental observations and theoretical principles to provide a comprehensive understanding of capillary pressure under varying temperature and saturation conditions. Furthermore, our model is not based on regression correlations and does not require any tuning factors. It can be universally applied to various rock types using just two sets of macroscopic (P_c^{ref}) and microscopic (IFT and θ) experimental data. In addition, the interfacial tension and contact angle measurements employed in our model are significantly more cost-effective and time-efficient

https://doi.org/10.1021/acs.est.5c08417
Environ. Sci. Technol. 2026, 60, 6149−6161

compared to the conventional approach of obtaining multiple P_c curves under different temperature conditions.

Although rock wettability affects both capillary pressure and relative permeability (K_r), the present study focuses on the temperature dependence of P_c while keeping K_r constant. This simplification was adopted to isolate the primary mechanism controlling CO_2 leakage and to avoid additional uncertainty introduced by the lack of reliable temperature-dependent K_r correlations for CO_2−water systems. It should be noted that neglecting the variation of K_r with temperature may lead to deviations in the simulated leakage, particularly in estimating the CO_2 migration rate through the caprock. Nevertheless, the leakage occurrence and total leaked mass are predominantly governed by P_c, and thus the conclusions drawn in this study remain valid. Future work should focus on incorporating temperature-dependent relative permeability modeling once sufficient experimental data become available, thereby improving the quantitative representation of the impact of wettability alteration on flow rate in CPG systems. Existing temperature-dependent oil−water relative permeability models developed for Steam-Assisted Gravity Drainage (SAGD) operations[47−49] might provide useful references for future model development.

2.3. CPG Simulation Cases and Rock Wettability Data

The CPG Simulation Model is a derivative version based on the SPE11C model,[50] modified and adapted to meet the specific needs of this study. The model scale has been reduced to 1008 m × 500 m × 360 m, which represents a typical size for CPG exploitation simulations. To enable CO_2 migration to the production well located in the upper part of the model, the impermeable layer in the middle of the model was replaced with a permeable aquifer. The caprock layer at the top of the model (Facies 1) was retained to prevent CO_2 from leaking out of the target formation. The grid model has dimensions of 168 × 25 × 100, and the formation exhibits anisotropy, with different layers having varying porosity and permeability.

Figure 2A illustrates the numerical grid model generated by our reservoir simulator, providing a detailed representation of the geological setup. The top boundary of the model (the top of Facies 1) is isobarically opened to simulate potential CO_2 leakage through caprock. The initial average temperature of the formation is 420 K, the average pressure is 200 bar, and the formation is saturated with hot brine. The injection wells consist of six horizontal wells aligned in the *Y*-direction, evenly distributed at the bottom of the high-permeability aquifer (Facies 5). Each injection well is 420 m in length and strategically spaced to maximize the sweep efficiency of CO_2. The wells inject CO_2 continuously at a rate of 905 tons per day. A single horizontal production well is located near the top of the aquifer, oriented in the *X*-direction. This well spans 960 m and operates under a constant bottom-hole pressure (BHP), which is equal to the initial well block pressure (185 bar). This BHP control ensures the continuous operation of the CPG system and maintains its stability. The injection rate in this study was determined through an iterative procedure that balances geothermal energy extraction efficiency and the usability of the recovered heat. Two operational constraints were imposed: (1) the total CPG operation period was set to 80 years and (2) the bottom-hole temperature (BHT) at the production well was designed to reach 328 K (55 °C) at the end of operation. An initial injection rate was first assigned, and the CO_2 cycling process was simulated for 80 years. If the simulated production well BHT after 80 years exceeded 55 °C, the injection rate was increased; otherwise, it was reduced. The target BHT of 328 K represents a balanced condition between energy recovery efficiency and the practical usability of the extracted heat. A higher terminal BHT would indicate incomplete thermal extraction, whereas a lower BHT would yield CO_2 at a temperature too low for practical utilization, even for district heating. The final injection rate derived from this procedure corresponds to a million-ton−scale CPG project (approximately 1.97 Mt yr^{-1}), consistent with the industrial expectations for large-scale CCUS deployment.[51] Further information about the CPG model can be found in Appendices A, B and C. After the geothermal extraction is terminated, we will simulate the subsequent migration of CO_2 within the reservoir for 2000 years to ensure that the CO_2 in the formation reaches equilibrium. The SPE11 project involved extensive intercomparison exercises among multiple research teams, focusing on coupled processes of CO_2 dissolution, multiphase flow, and heat transport in geological formations. As a participant in the SPE11 benchmark project, we published comparative results with other teams,[52] providing validation for the numerical framework adopted in this study. The CPG reservoir model established here is based on the SPE11C configuration, ensuring that the above validation is still applicable to the present simulations.

The wettability data for our CPG simulations consist of four key components: relative permeability curves, capillary pressure curve at a reference temperature, contact angle at different temperatures and interfacial tension (IFT) at different temperatures. The relative permeability curves and capillary pressure at reference temperature were determined using empirical formulas that are suggested in the SPE11 project. For relative permeability, the Brooks-Corey model was applied.[37] This model uses normalized saturations to calculate phase permeabilities, accounting for immobile phase saturations in the normalization process. The formula includes parameters that define the nonlinearity of the relationship between relative permeability and saturation. Similarly, the capillary pressure curve is also based on the Brooks-Corey equation, incorporating entry pressure and normalized water saturation. The extended capillary pressure model accounts for maximum capillary pressure using an error function to ensure smooth transitions, making it suitable for multiphase flow scenarios. The contact angle at different temperatures and the IFT data were obtained from literature, specifically from measurements on a shale sample.[26] This type of rock, with its excellent compactness, is suitable for use as a caprock in the CPG model. To provide a more intuitive understanding of these data sets, we have plotted the Facies 1 (caprock) data in Figure 2B. Since capillary pressure in the storage formation has a negligible effect on CO_2 leakage, this study focuses only on the thermal effect on the caprock. Therefore, contact angle and interfacial tension data for other facies are not required. The corresponding capillary pressure, relative permeability, contact angle and IFT data for all facies are provided in Appendix D for reference.

It should be noted that the simulation results depend on several key input parameters, including the interfacial tension (IFT), contact angle, injection type, and well configuration. In this study, these parameters were selected based on representative experimental correlations and typical CPG operation schemes. While variations in these inputs may affect the quantitative results, the modeling framework and findings

https://doi.org/10.1021/acs.est.5c08417
Environ. Sci. Technol. 2026, 60, 6149−6161

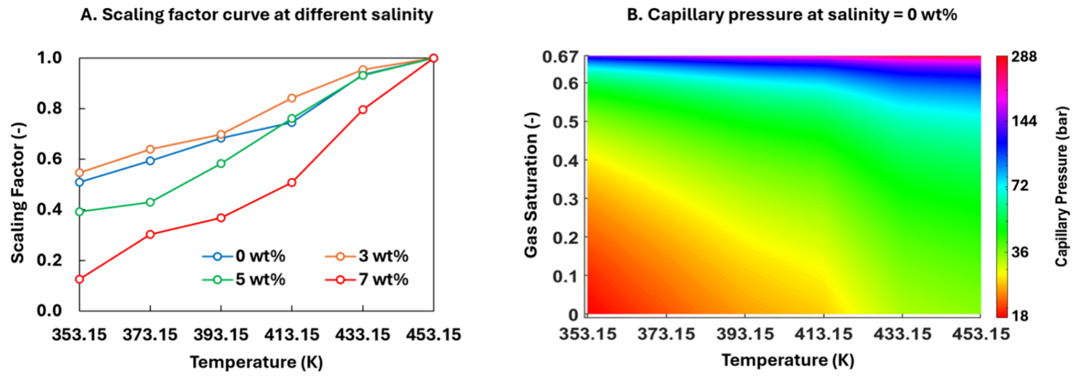

Figure 3. Calculated scaling factor and capillary pressure from the TSPC model.

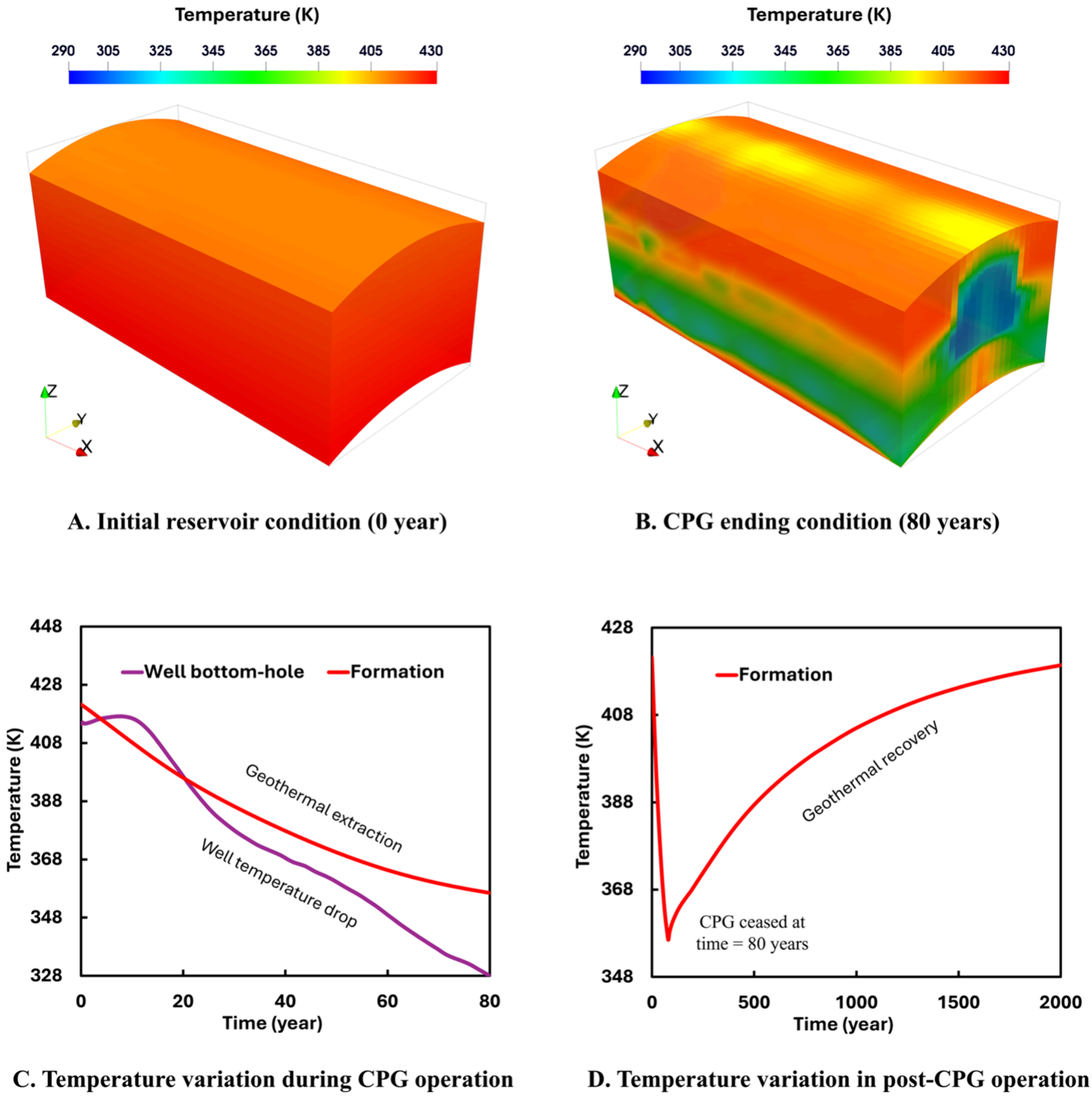

Figure 4. Formation and production well bottom-hole temperature evolution from CPG simulations.

https://doi.org/10.1021/acs.est.5c08417
Environ. Sci. Technol. 2026, 60, 6149−6161

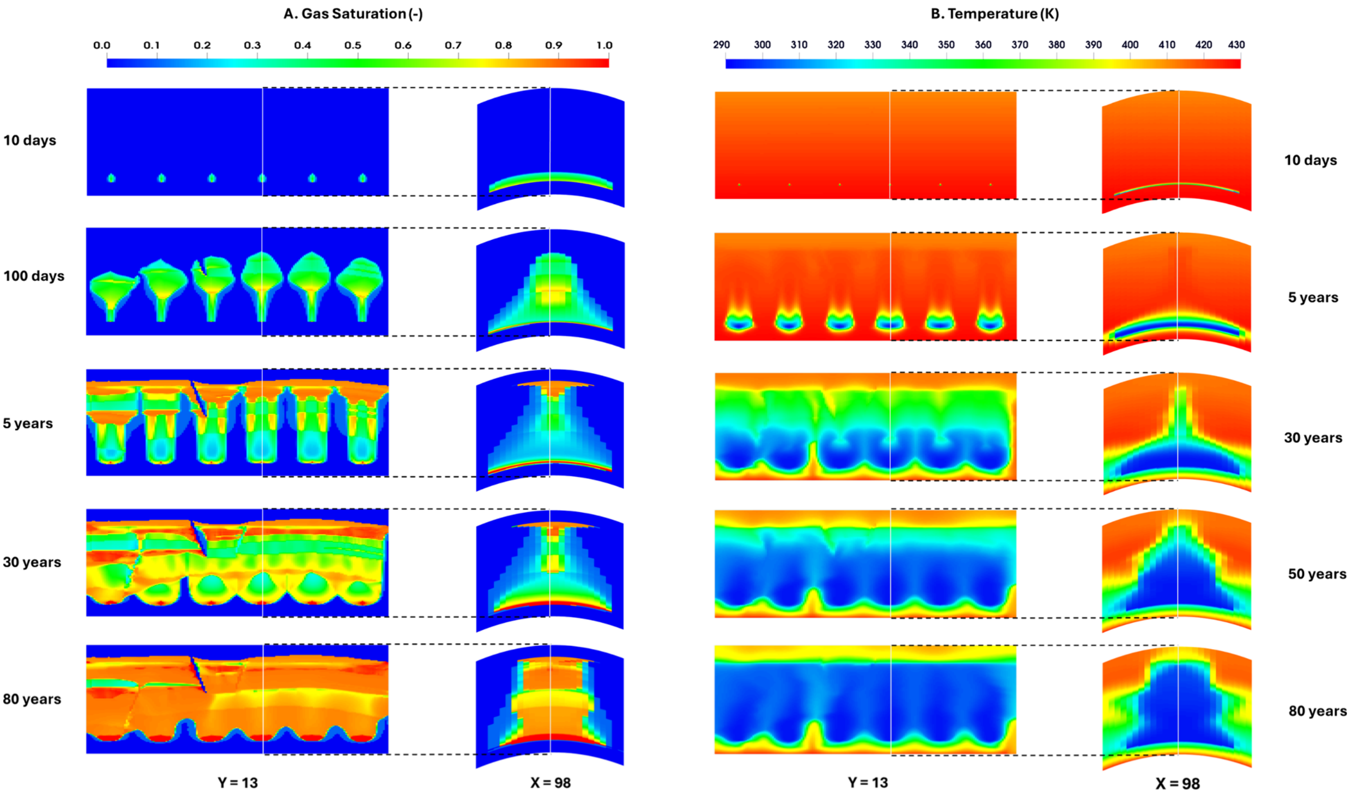

Figure 5. Cross-sectional views of gas (CO_2-rich) phase distribution and temperature variation during a CPG operation.

remain valid for conventional CPG projects. For nonstandard CPG operations, specific model settings may need to be adjusted to improve simulation accuracy and ensure reliable prediction.

3. RESULTS AND DISCUSSIONS

This section presents the key findings of our study, divided into two parts. The first part focuses on the results of capillary pressure modeling, highlighting the impact of temperature variations on capillary sealing capacity. The second part extends the analysis to field-scale CPG numerical simulations, investigates the effects of temperature reduction during geothermal extraction on the capillary sealing capacity of caprock and assesses the potential risks of CO_2 leakage.

3.1. Capillary Pressure Modeling Results

The TSPC model was utilized to calculate scaling factor curves and capillary pressure values under varying temperature and gas saturation conditions. These calculations were based on the wettability data presented in Figure 2B. In Figure 3A, the scaling factor curves generated from the TSPC model highlight the effects of temperature and salinity. The results show that the scaling factor decreases with reduced temperatures. In contrast, salinity exerts a complex influence on the scaling factor, with higher salinity generally leading to a smaller scaling factor. According to eq 7, the scaling factor is directly proportional to capillary pressure, indicating that capillary pressure tends to increase as temperature rises. As the temperature decreases from 180 to 80 °C, the capillary pressure is reduced to approximately 13% to 55% of its original value, depending on the salinity level. This trend is validated by the simulation results of capillary pressure presented in Figure 3B, which shows the calculated capillary pressure under varying temperature and saturation conditions. The results confirm that capillary pressure decreases with falling temperature, consistent with the scaling factor trends observed in Figure 3A.

In caprock formations, capillary pressure acts as a key barrier that prevents the upward migration of buoyant CO_2. It is strongly influenced by wettability, which controls the fluid-rock contact angle. When the caprock is strongly water-wet, the capillary entry pressure is high, making it more difficult for CO_2 to access the pore throats of the rock. However, according to the above results, cooling-induced wettability alteration reduces the rock's affinity for water, which effectively lowers the capillary pressure. As a result, CO_2 can enter it more easily and migrate through the caprock pores, undermining the effectiveness of its capillary seal. This process compromises the integrity of geological CO_2 sequestration and raises concerns about long-term safety, particularly in systems where temperature variations are significant, such as in CO_2 plume geothermal (CPG) operations. The results in Figure 3 quantify the impact of temperature-induced wettability alterations on the capillary sealing capacity of rocks, providing a theoretical basis for the following field-scale CPG simulations. In the CPG simulations, the data obtained from Figure 3B will be used to model the capillary pressure in the formation as a function of both temperature and saturation, so that it can capture the thermal effect. This approach allows for a more realistic representation of reservoir conditions and facilitates a more accurate assessment of CO_2 migration and potential leakage during both geothermal energy extraction and the post-CPG sequestration phase.

3.2. Field-Scale CPG System Simulations

To establish a basic understanding of the CO_2 plume geothermal (CPG) systems, we conducted simulations excluding the impact of temperature reduction on capillary

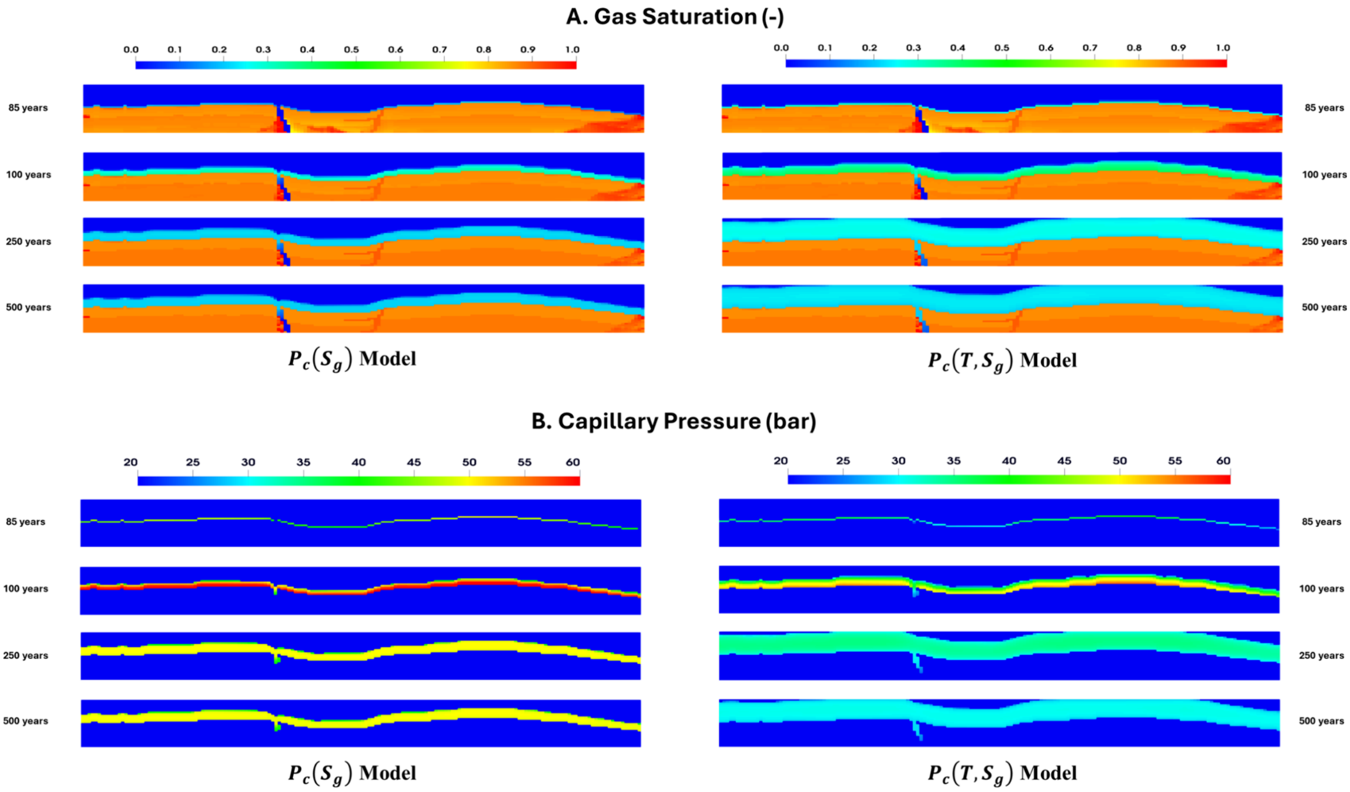

Figure 6. Comparison of CO_2 migration and capillary pressure distribution in the caprock during the post-CPG period with and without considering thermal effect.

pressure. This provides insights into the migration of subsurface fluids during the operation of a field-scale CPG project.

Figure 4 illustrates the evolution of formation and production well bottom-hole temperature before and after the operation of a CO_2 Plume Geothermal (CPG) system. Initially, the formation exhibits a relatively high and uniform temperature distribution, indicating that the reservoir contains considerable geothermal resources and is an ideal candidate for CPG exploitation. After CPG operation (t = 80 years), a pronounced reduction in formation temperature is observed in most regions of the reservoir (Figure 4B). Figure 4C quantitatively illustrates the temporal evolution of formation and well temperatures during the 80-year operation period. The average formation temperature decreases from approximately 421 to 356 K, corresponding to a reduction of about 65 K. The well bottom-hole temperature drops more significantly, reaching 328 K at the end of the operation. This value is consistent with the design constraint specified in Section 2.3, confirming that further operation would yield negligible geothermal benefit and can thus be terminated. After shut-in, Figure 4D depicts the subsequent geothermal recovery process. The temperature recovery is extremely slow, taking thousands of years for the formation to approach its initial temperature. This prolonged low-temperature state implies that the capillary sealing capacity of caprock remains partially weakened for an extended period, thereby increasing the potential risk of CO_2 leakage before full thermal recovery is achieved.

Figure 5A presents cross-sectional views of the gas phase (CO_2-rich phase) distribution over time, corresponding to the simulation model shown in Figure 4. Both panels display vertical slices at specific times, with the left panel showing the cross-section at $Y = 13$ and the right panel depicting the cross-section at X = 98. Initially, the gas phase appears around the injection wells due to the CO_2 injection (t = 10 days). Driven by the pressure difference between the injection wells and the production well in the upper area of the model, as well as the density difference between gas and water, the injected CO_2 migrates upward and forms several distinct CO_2 plumes (t = 100 days). As the injection progresses, the CO_2 plumes expand and eventually surround the production wells, making CO_2 become the primary heat-carrying fluid (t = 5 years). As the sustained operation of the CPG system, the CO_2 plumes further grow and merge into a single, continuous plume. The gas phase saturation increases significantly due to the formation water being gradually extracted, as shown at t = 30 years and t = 80 years. Notably, CO_2 leakage is not observed during the operation, which can be attributed to the low-pressure region around the production wells and the sealing integrity of the caprock. However, the accumulation of CO_2 beneath the caprock poses a potential risk for upward migration during the post-CPG period. As the formation temperature gradually recovers after CPG shut-in, the thermal expansion of CO_2 may lead to an increase in reservoir pressure, potentially enabling CO_2 to overcome capillary entry pressures and migrate through the caprock, thereby compromising long-term storage security. Therefore, maintaining good sealing integrity of the caprock over the entire storage lifespan is essential for ensuring the safety and effectiveness of CO_2 sequestration in the post-CPG period.

Figure 5B illustrates the temporal evolution of the temperature field within the reservoir during the operation of the CPG system, presented as cross-sectional views. Both

https://doi.org/10.1021/acs.est.5c08417
Environ. Sci. Technol. 2026, 60, 6149−6161

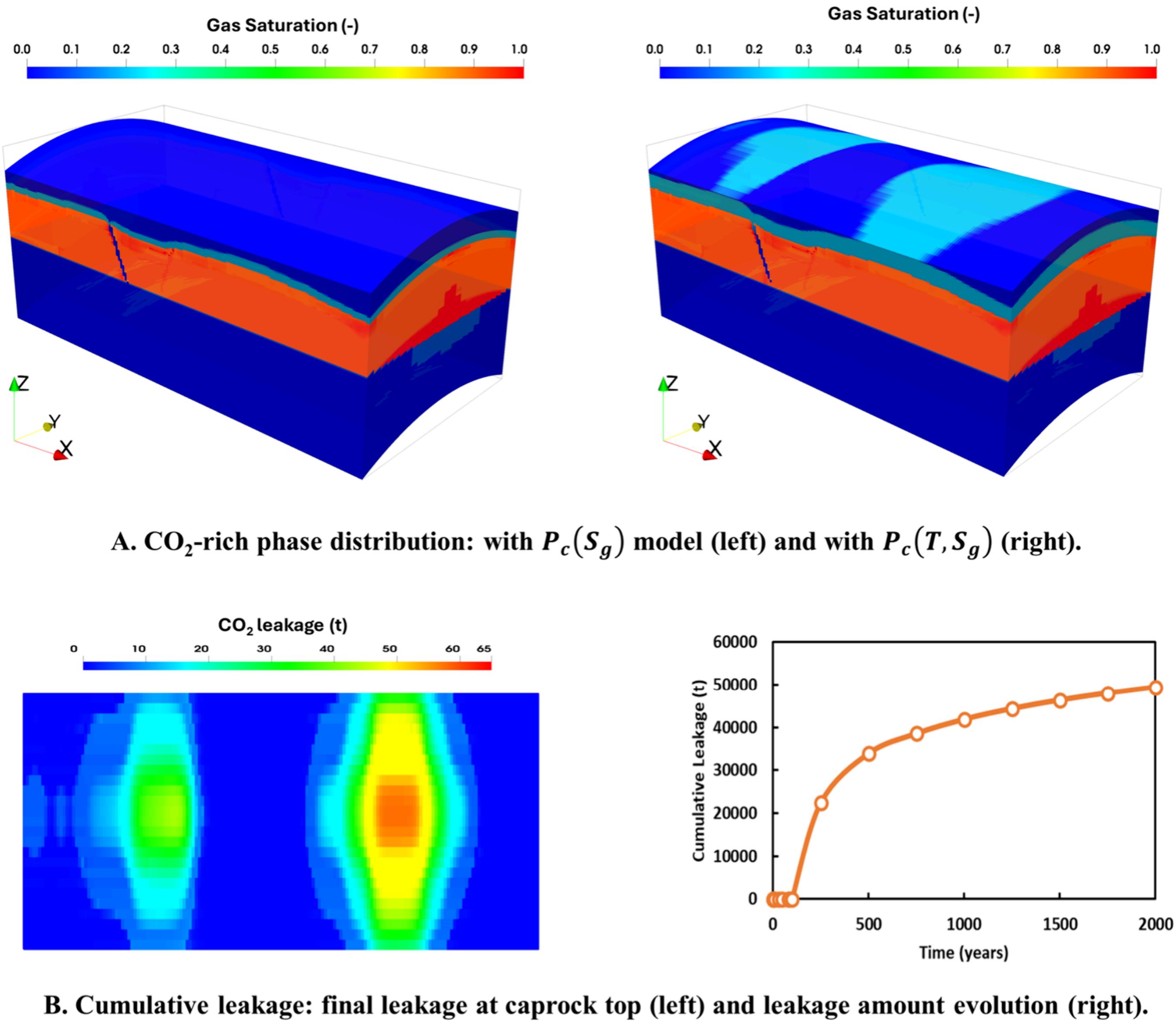

Figure 7. CO_2 leakage distribution and cumulative leakage during the post-CPG period with cooling-induced capillary pressure reduction.

panels display vertical slices, with the left panel showing the cross-section at $Y = 13$ and the right panel depicting the cross-section at X = 98. At the initial stage, the temperature distribution is relatively uniform, reflecting a constant geothermal reservoir gradient. As CO_2 injection and heat production progress, localized cooling zones begin to form around the injection wells due to the injection of cool CO_2. By t = 5 years, distinct regions of lower temperature can be observed, indicating that heat from these areas has already been transported by CO_2 to the top of the model or extracted to the surface. With the sustained CO_2 injection, the cooling effect becomes more pronounced (t = 30 years). Over time, these cooling zones expand laterally and vertically, eventually covering most of the reservoir area near the production wells (t = 50 years). Unlike the changes in gas phase saturation, the temperature field evolves more rapidly in the horizontal direction, with several low-temperature regions merging quickly. However, in the vertical direction, the expansion of the low-temperature zones is much slower, allowing the production area to maintain high temperatures for a relatively long period, which is beneficial for geothermal energy extraction. By t = 80 years, the temperature field shows significant cooling in most of the geothermal reservoirs, indicating that the geothermal resources have been effectively extracted. Meanwhile, the low-temperature front reaches the production well, resulting in a noticeable drop in the fluid temperature within the wellbore. Once the temperature falls below the predefined shut-in threshold (t < 328 K), CPG operations are terminated (almost at t = 80 years), and the simulation transitions into the post-CPG period focused on geological CO_2 storage. The cross-sectional views in Figure 5 provide a detailed visualization of CO_2 distribution and temperature variation within the subsurface formation, offering a deep understanding of its migration behavior during CPG system operation. These insights pave the way for subsequent investigations into cooling-induced CO_2 leakage. Additionally, the results show that most of the high-temperature regions are affected and exhibit significant temperature reductions, further highlighting the high efficiency of the CO_2 plume in facilitating thermal energy extraction.

https://doi.org/10.1021/acs.est.5c08417
Environ. Sci. Technol. 2026, 60, 6149−6161

The TSPC model ($P_c[T, S_g]$) proposed in this study is further applied to conduct the same CPG simulation to evaluate the impact of cooling-induced wettability alteration on capillary sealing capacity. During the operational phase of the CPG system, the simulation results are consistent with those obtained using the conventional saturation-dependent capillary pressure model ($P_c[S_g]$). However, significant differences emerge during the post-CPG carbon storage phase, particularly in the CO_2 migration within the caprock. Figure 6 presents a comparison of CO_2 distribution and capillary pressure in the caprock during the post-CPG period. The figure illustrates a vertical cross-section within the upper part of the model (Y = 13, Z < 28), focusing on the interior of the caprock. Following the cessation of CPG operations, residual heat within the formation is gradually absorbed by the CO_2, leading to thermal expansion and a consequent increase in reservoir pressure. This pressure buildup drives CO_2 upward, initiating its migration into the overlying caprock in both cases around 85−100 years. Once the gas phase enters the caprock, capillary pressure appears and resists further CO_2 migration. This behavior is clearly observed in Figure 6B, where regions containing gaseous CO_2 exhibit elevated capillary pressure, effectively hindering further upward migration and potential leakage. However, when temperature-induced wettability alteration is taken into account using the TSPC model (right column of Figure 6, the capillary pressure values are substantially lower than those predicted by the conventional model (left column). This reduction in capillary pressure compromises the sealing capacity of the caprock and increases the risk of CO_2 leakage. This concern is further substantiated by simulation results in an extended post-CPG period (250−500 years). As shown in the left panels, CO_2 remains effectively trapped within the caprock, ensuring secure long-term storage. In contrast, in the right panels where temperature effects on capillarity are considered, CO_2 breaches the caprock and migrates beyond the upper boundary of the model, indicating CO_2 is leaked from the target sequestration formation.

Through the above discussion, we have examined the internal evolution of the gas saturation and formation temperature and explained the underlying mechanisms of cooling-induced CO_2 leakage. Building on these analyses, we will further investigate the spatial characteristics and magnitude of CO_2 leakage. Figure 7 presents the leakage distribution at the top domain of the model as well as the cumulative leakage amount over time. As shown in Figure 7A, gas-phase CO_2 appears near the top boundary of the model when the thermal effect on capillary pressure is considered, with a portion of the gas leaking beyond the target sequestration formation. In contrast, no leakage is observed in the case where temperature effects on capillary pressure are neglected. Similarly, previous studies on CO_2 leakage risk assessment have shown that reduced capillary pressure weakens caprock sealing capacity and facilitates CO_2 and leakage.[53−55] These findings support our simulation results, which indicate that cooling-induced capillary pressure reduction leads to increased leakage risk. Figure 7B depicts the spatial distribution of CO_2 leakage along the top boundary, which closely aligns with regions of high gas saturation. This indicates that CO_2 primarily leaks in the form of free gas, whereas dissolved CO_2 is securely trapped within the formation. The cumulative leakage curve in the lower right panel quantitatively illustrates the leakage amount over time. During the postinjection period, nearly 50,000 tons of CO_2 are observed to leak out from the caprock, raising serious concerns regarding long-term storage security. In original SPE11 benchmark simulations from previous research,[52] the caprock successfully contained CO_2 without any leakage. In contrast, when the cooling effect is introduced in this study, the capillary sealing capacity is significantly reduced, leading to clear CO_2 breakthrough near the top of the model. These results demonstrate that cooling-induced wettability alteration represents a critical mechanism that can undermine caprock integrity, yet it has been largely overlooked in previous CPG research. Neglecting these factors may lead to a significant underestimation of leakage risks and compromise the safety and capacity of these dual-purpose systems.

4. IMPLICATIONS

This study investigates the impact of cooling-induced wettability alteration on the capillary sealing capacity of caprock in CO_2−Plume Geothermal (CPG) systems associated with geological CO_2 sequestration. The capillary pressure between CO_2 and water can inhibit further upward migration. However, the long-term sealing effectiveness depends on whether the capillary pressure is sufficient to withstand the pressure differential induced by CO_2 thermal expansion. A temperature-sensitive capillary pressure model is proposed and applied to simulate the dynamic alteration in capillary pressure under varying thermal conditions. For the caprock samples used in this study, a temperature decrease from 453.15 to 353.15 K resulted in a capillary pressure reduction ranging from 45% to 87%. The above cooling-induced reduction in capillary pressure can severely impair the sealing capacity of the caprock. In our field-scale CPG simulations, approximately 50,000 tons of CO_2 escaped from the target formation when thermal effects on capillary pressure were considered. Most of the leakage occurs in the supercritical CO_2 phase, while the dissolved CO_2 remains securely trapped within the formation. In summary, the primary mechanism of cooling-induced CO_2 leakage lies in the reduction of capillary sealing capacity caused by caprock wettability alteration. As the formation temperature decreases during CPG operation, the reduced capillary pressure facilitates upward migration of gas-phase CO_2, eventually leading to the leakage. Such leakage can have severe environmental implications: the upward migration of CO_2 may eventually be released into the atmosphere, reducing the overall effectiveness of carbon sequestration efforts; there is a potential risk of freshwater contamination if CO_2 intrudes into shallower freshwater aquifers, reducing potable water supplies.

To mitigate the risk of cooling-induced CO_2 leakage, several mitigation strategies are proposed and discussed below. (1) Optimization of injection and production schemes: adjusting injection−production schedules can effectively mitigate local cooling intensity near the caprock and help preserve its capillary sealing capacity. This approach is particularly effective when the cooling zone overlaps with the caprock region; however, it may require limiting the development area adjacent to the caprock, thereby reducing overall geothermal extraction efficiency. Before implementing this strategy, CPG numerical simulations should be carried out to evaluate the economic feasibility of the associated reduction in geothermal energy recovery. (2) Reducing caprock leakage risk through site selection: selecting CPG sites with good connectivity to large, permeable aquifers can effectively dissipate the pressure buildup associated with CO_2 thermal expansion in the post-CPG period. This strategy reduces the pressure differential

https://doi.org/10.1021/acs.est.5c08417
Environ. Sci. Technol. 2026, 60, 6149−6161

between the reservoir and the caprock, thereby lowering the driving force for upward CO_2 migration. With a decreased driving force, the risk of CO_2 leakage can remain well controlled even if the caprock sealing capacity is partially weakened. This strategy requires more detailed geological and hydrodynamic information to accurately characterize hydraulic connectivity. These data sets should cover not only the reservoir and caprock but also the laterally and vertically connected aquifer systems at the reservoir boundaries. Furthermore, the strict site-selection requirements significantly decrease the number of suitable sites for CPG application, limiting its large-scale applicability. (3) Pressure management wells: a production well can be placed at the bottom of the reservoir to withdraw formation water after CPG operation. Continuous or intermittent production of formation water from the reservoir bottom can relieve pressure caused by CO_2 expansion during the postoperation period. However, this strategy also poses two major challenges. First, because the geothermal recovery process may last for thousands of years, the pressure management wells would need to operate over an extended period with slow water withdrawal, significantly increasing maintenance and operational costs. Second, maintaining active production wells for such a long duration also raises safety risks, which must be carefully managed during postoperation monitoring and control.

■ ASSOCIATED CONTENT

Supporting Information

The Supporting Information is available free of charge at https://pubs.acs.org/doi/10.1021/acs.est.5c08417.

Appendix A: Geological data; Appendix B: Well data; Appendix C: Fluid data; Appendix D: Wettability data (PDF)

■ AUTHOR INFORMATION

Corresponding Authors

Fei Tian − *Key Laboratory of Deep Petroleum Intelligent Exploration and Development, Institute of Geology and Geophysics, Chinese Academy of Sciences, Beijing 100029, China; College of Earth and Planetary Sciences, University of Chinese Academy of Sciences, Beijing 100049, China;* Email: tianfei@mail.iggcas.ac.cn

Liang Zhao − *Key Laboratory of Deep Petroleum Intelligent Exploration and Development, Institute of Geology and Geophysics, Chinese Academy of Sciences, Beijing 100029, China; College of Earth and Planetary Sciences, University of Chinese Academy of Sciences, Beijing 100049, China;* Email: zhaoliang@mail.iggcas.ac.cn

Zhangxin Chen − *Ningbo Institute of Digital Twin, Eastern Institute of Technology, Ningbo 315200, China; Department of Chemical and Petroleum Engineering, University of Calgary, Calgary T2N1N4, Canada;* orcid.org/0000-0002-9107-1925; Email: zhachen@ucalgary.ca

Authors

Chaojie Di − *Key Laboratory of Deep Petroleum Intelligent Exploration and Development, Institute of Geology and Geophysics, Chinese Academy of Sciences, Beijing 100029, China; College of Earth and Planetary Sciences, University of Chinese Academy of Sciences, Beijing 100049, China*

Peng Deng − *Department of Chemical and Petroleum Engineering, University of Calgary, Calgary T2N1N4, Canada*

Haoming Ma − *School of Energy Resources, University of Wyoming, Laramie, Wyoming 82071, United States*

Benjieming Liu − *Ningbo Institute of Digital Twin, Eastern Institute of Technology, Ningbo 315200, China;* orcid.org/0000-0001-8674-2176

Long Peng − *CNPC R&D (DIFC) Company Limited, Dubai 415147, UAE*

Complete contact information is available at: https://pubs.acs.org/10.1021/acs.est.5c08417

Notes

The authors declare no competing financial interest.

■ ACKNOWLEDGMENTS

This study was supported by the CAS Project for Young Scientists in Basic Research (YSBR-020) and the Energi Simulation (365863-17).

■ REFERENCES

(1) Zimmerman, J. B.; Anastas, P. T.; Erythropel, H. C.; Leitner, W. Designing for a Green Chemistry Future. *Science (1979)* **2020**, *367* (6476), 397−400.

(2) Deng, P.; Chen, Z.; Peng, X.; Zhu, S.; Liu, B.; Lei, X.; Di, C. Converting Underground Natural Gas Storage for Hydrogen: A Review of Advantages, Challenges and Economics. *Renewable and Sustainable Energy Reviews* **2025**, *213*, No. 115438.

(3) Liu, L.; Miranda, M. M.; Bielicki, J. M.; Ellis, B. R.; Johnson, J. X. Life Cycle Greenhouse Gas Emissions of CO2-Enabled Sedimentary Basin Geothermal. *Environ. Sci. Technol.* **2024**, *58* (4), 1882−1893.

(4) Yang, X.; Jiang, X.; Liang, S.; Qin, Y.; Ye, F.; Ye, B.; Xu, J.; He, X.; Wu, J.; Dong, T.; Cai, X.; Xu, R.; Zeng, Z. Spatiotemporal Variation of Power Law Exponent on the Use of Wind Energy. *Appl. Energy* **2024**, *356*, No. 122441.

(5) International Energy Agency *Future of Geothermal Energy* 2024 https://www.iea.org/reports/the-future-of-geothermal-energy

(6) McQueen, N.; Psarras, P.; Pilorgé, H.; Liguori, S.; He, J.; Yuan, M.; Woodall, C. M.; Kian, K.; Pierpoint, L.; Jurewicz, J.; Lucas, J. M.; Jacobson, R.; Deich, N.; Wilcox, J. Cost Analysis of Direct Air Capture and Sequestration Coupled to Low-Carbon Thermal Energy in the United States. *Environ. Sci. Technol.* **2020**, *54* (12), 7542−7551.

(7) Dai, Q.; Zhang, L.; Zhang, K.; Chen, G.; Chen, Z.; Xue, X.; Wang, Y.; Wang, Z.; Di, C.; Zhao, F.; Bai, J. Carbon-Pricing Optimization Framework for Oilfield Carbon Dioxide-Water Alternation with Economic and Environmental Gains. *Energy Convers. Manag.* **2026**, *348*, No. 120613.

(8) Sharmin, T.; Khan, N. R.; Akram, M. S.; Ehsan, M. M. A State-of-the-Art Review on Geothermal Energy Extraction, Utilization, and Improvement Strategies: Conventional, Hybridized, and Enhanced Geothermal Systems. *International Journal of Thermofluids* **2023**, *18*, No. 100323.

(9) Xue, Z.; Ma, H.; Wei, Y.; Wu, W.; Sun, Z.; Chai, M.; Zhang, C.; Chen, Z. Integrated Technological and Economic Feasibility Comparisons of Enhanced Geothermal Systems Associated with Carbon Storage. *Appl. Energy* **2024**, *359*, No. 122757.

(10) Liu, Y.; Hu, T.; Rui, Z.; Zhang, Z.; Du, K.; Yang, T.; Dindoruk, B.; Halfdan Stenby, E.; Torabi, F.; Afanasyev, A. An Integrated Framework for Geothermal Energy Storage with CO2 Sequestration and Utilization. *Engineering* **2023**, *30*, 121−130.

(11) Yalcin, B.; Ezekiel, J.; Mai, P. M. Potential for CO2 Plume Geothermal and CO2 Storage in an Onshore Red Sea Rift Basin, Al-Wajj, Saudi Arabia: 3D Reservoir Modeling and Simulations. *Geothermics* **2024**, *119*, No. 102966.

(12) Cui, G.; Ren, S.; Rui, Z.; Ezekiel, J.; Zhang, L.; Wang, H. The Influence of Complicated Fluid-Rock Interactions on the Geothermal Exploitation in the CO2 Plume Geothermal System. *Appl. Energy* **2018**, *227*, 49−63.

(13) Seto, C. J.; McRae, G. J. Reducing Risk in Basin Scale CO2 Sequestration: A Framework for Integrated Monitoring Design. *Environ. Sci. Technol.* **2011**, *45* (3), 845−859.

(14) Fitts, J. P.; Peters, C. A. Caprock Fracture Dissolution and CO2 Leakage. *Rev. Mineral. Geochem.* **2013**, *77* (1), 459−479.

(15) Rizzo, R. E.; Inskip, N. F.; Fazeli, H.; Betlem, P.; Bisdom, K.; Kampman, N.; Snippe, J.; Senger, K.; Doster, F.; Busch, A. Modelling Geological CO2 Leakage: Integrating Fracture Permeability and Fault Zone Outcrop Analysis. *International Journal of Greenhouse Gas Control* **2024**, *133*, No. 104105.

(16) Wang, Z.; Li, H.; Liu, S.; Xu, J.; Liu, J.; Wang, X. Risk Evaluation of CO2 Leakage through Fracture Zone in Geological Storage Reservoir. *Fuel* **2023**, *342*, No. 127896.

(17) Zhang, L.; Yang, Q.; Jiang, M.; Yang, W.; Bian, Y. A New Salt-Precipitation-Based Self-Remediation Model for CO2 Leakage along Fault during Geological CO2 Storage. *Energy* **2024**, *305*, No. 132286.

(18) Zhang, L.; Zhang, S.; Jiang, W.; Wang, Z.; Li, J.; Bian, Y. A Mechanism of Fluid Exchange Associated to CO2 Leakage along Activated Fault during Geologic Storage. *Energy* **2018**, *165*, 1178−1190.

(19) Cai, Y.; Yang, D.; Feng, G.; Lei, H. Transient H2O−CO2 Wellbore Leakage under Evolving Recharge Conditions Considering CO2 Phase Change. *J. Clean. Prod.* **2024**, *450*, No. 141942.

(20) Dai, Z.; Viswanathan, H.; Middleton, R.; Pan, F.; Ampomah, W.; Yang, C.; Jia, W.; Xiao, T.; Lee, S.-Y.; McPherson, B.; Balch, R.; Grigg, R.; White, M. CO2 Accounting and Risk Analysis for CO2 Sequestration at Enhanced Oil Recovery Sites. *Environ. Sci. Technol.* **2016**, *50* (14), 7546−7554.

(21) Gupta, P. K.; Yadav, B. Leakage of CO2 from Geological Storage and Its Impacts on Fresh Soil−Water Systems: A Review. *Environmental Science and Pollution Research* **2020**, *27* (12), 12995−13018.

(22) Di, C.; Wei, Y.; Wang, K.; Deng, P.; Chen, B.; Shen, L.; Chen, Z. The Impact of Pressurization-Induced Decrease of Capillary Pressure and Residual Saturation on Geological Carbon Dioxide Storage. *J. Clean. Prod.* **2025**, *486*, No. 144573.

(23) Plug, W. J.; Bruining, J. Capillary Pressure for the Sand-CO2-Water System under Various Pressure Conditions. Application to CO2 Sequestration. *Adv. Water Resour.* **2007**, *30* (11), 2339−2353.

(24) Al-Yaseri, A. Z.; Lebedev, M.; Barifcani, A.; Iglauer, S. Receding and Advancing (CO2+ Brine + Quartz) Contact Angles as a Function of Pressure, Temperature, Surface Roughness, Salt Type and Salinity. *J. Chem. Thermodyn.* **2016**, *93*, 416−423.

(25) Arif, M.; Al-Yaseri, A. Z.; Barifcani, A.; Lebedev, M.; Iglauer, S. Impact of Pressure and Temperature on CO2-Brine-Mica Contact Angles and CO2-Brine Interfacial Tension: Implications for Carbon Geo-Sequestration. *J. Colloid Interface Sci.* **2016**, *462*, 208−215.

(26) Yekeen, N.; Padmanabhan, E.; Abdulelah, H.; Irfan, S. A.; Okunade, O. A.; Khan, J. A.; Negash, B. M. CO2/Brine Interfacial Tension and Rock Wettability at Reservoir Conditions: A Critical Review of Previous Studies and Case Study of Black Shale from Malaysian Formation. *J. Pet. Sci. Eng.* **2021**, *196*, No. 107673.

(27) Sarmadivaleh, M.; Al-Yaseri, A. Z.; Iglauer, S. Influence of Temperature and Pressure on Quartz−Water−CO2 Contact Angle and CO2−Water Interfacial Tension. *J. Colloid Interface Sci.* **2015**, *441*, 59−64.

(28) Singh, D.; Friis, H. A.; Jettestuen, E.; Helland, J. O. Ripening of Capillary-Trapped CO2 Ganglia Surrounded by Oil and Water at the Pore Scale: Impact of Reservoir Pressure and Wettability. *Energy Fuels* **2024**, *38* (10), 8853−8874.

(29) Zhou, Y.; Hatzignatiou, D. G.; Helland, J. O. On the Estimation of CO2 Capillary Entry Pressure: Implications on Geological CO2 Storage. *International Journal of Greenhouse Gas Control* **2017**, *63*, 26−36.

(30) Andrew, M.; Bijeljic, B.; Blunt, M. J. Pore-by-Pore Capillary Pressure Measurements Using X-Ray Microtomography at Reservoir Conditions: Curvature, Snap-off, and Remobilization of Residual CO2. *Water Resour. Res.* **2014**, *50* (11), 8760−8774.

(31) Garing, C.; de Chalendar, J. A.; Voltolini, M.; Ajo-Franklin, J. B.; Benson, S. M. Pore-Scale Capillary Pressure Analysis Using Multi-Scale X-Ray Micromotography. *Adv. Water Resour.* **2017**, *104*, 223−241.

(32) Kasha, A. A.; Sakhaee-Pour, A.; Hussein, I. A. Machine Learning for Capillary Pressure Estimation. *SPE reservoir evaluation & engineering* **2022**, *25* (1), 1−20.

(33) Khosravi, R.; Simjoo, M.; Chahardowli, M. Low Salinity Water Flooding: Estimating Relative Permeability and Capillary Pressure Using Coupling of Particle Swarm Optimization and Machine Learning Technique. *Sci. Rep.* **2024**, *14* (1), 13213−13215.

(34) CMG Ltd [Software] *CMG-STARTS* (Version 2025.20); CMG Ltd.: Calgary, 2025, https://www.cmgl.ca/

(35) SLB Ltd [Software] *ECLIPSE 100* (Version 2022.10) 2022. https://www.slb.com/products-and-services/delivering-digital-at-scale/software/eclipse-industry-reference-reservoir-simulator/eclipse

(36) Van Genuchten, M. A Closed-Form Equation for Predicting the Hydraulic Conductivity of Unsaturated Soils1. *Soil Science Society of America Journal* **1980**, *44* (5), 892−898.

(37) Brooks, R. H. *Hydraulic Properties of Porous Media*; Colorado State University: CO, 1965.

(38) Ren, B.; Littlefield, J.; Jia, C.; Ni, H.; Duncan, I. Impact of Pressure-Dependent Interfacial Tension and Contact Angle on Capillary Heterogeneity Trapping of CO2 in Storage Aquifers. *SPE Journal* **2024**, *29* (08), 4442−4458.

(39) Di, C.; Wei, Y.; Wang, K.; Liu, B.; Deng, P.; Sun, Z.; Lei, X.; Chen, Z. A Parallel Compositional Reservoir Simulator for Large-Scale CO2 Geological Storage Modeling and Assessment. *Science of The Total Environment* **2024**, *955*, No. 177065.

(40) Søreide, I.; Whitson, C. H. Peng-Robinson predictions for hydrocarbons, CO2, N2, and H2 S with pure water and NaCI brine. *Fluid Phase Equilib.* **1992**, *77*, 217−240.

(41) Liu, Z.; Cui, P.; Cui, X.; Wang, X.; Du, D. Prediction of CO2 Solubility in NaCl Brine under Geological Conditions with an Improved Binary Interaction Parameter in the Søreide-Whitson Model. *Geothermics* **2022**, *105*, No. 102544.

(42) National Institute of Standards and Technology *NIST (National Institute of Standards and Technology) Chemistry WebBook* https://webbook.nist.gov/chemistry/

(43) CMG Ltd *Get the clarity you need to make business critical decisions about your reservoir assets* 2025 https://www.cmgl.ca/

(44) SLB Ltd *Eclipse reservoir simulator* 2022 https://www.slb.com/products-and-services/delivering-digital-at-scale/software/eclipse-industry-reference-reservoir-simulator/eclipse

(45) Rock Flow Dynamics *Reservoir Modelling Software* 2024 https://rfdyn.com/

(46) Chen, Z.; Huan, G.; Ma, Y. *Computational Methods for Multiphase Flows in Porous Media*; Society for Industrial and Applied Mathematics, 2006.

(47) Esmaeili, S.; Sarma, H.; Harding, T.; Maini, B. Correlations for Effect of Temperature on Oil/Water Relative Permeability in Clastic Reservoirs. *Fuel* **2019**, *246*, 93−103.

(48) Hamouda, A. A.; Karoussi, O.; Chukwudeme, E. A. Relative Permeability as a Function of Temperature, Initial Water Saturation and Flooding Fluid Compositions for Modified Oil-Wet Chalk. *J. Pet. Sci. Eng.* **2008**, *63*, 61−72.

(49) Zeidani, M.; Maini, B. B. SAGD Relative Permeability as a Function of Temperature. In *SPE Canada Heavy Oil Technical Conference*; SPE, 2016, pp 7−9. DOI: .

(50) Nordbotten, J. M.; Ferno, M. A.; Flemisch, B.; Kovscek, A. R.; Lie, K.-A. The 11th Society of Petroleum Engineers Comparative Solution Project: Problem Definition. *SPE J.* **2024**, *29*, 2507−2524.

(51) Global CCS Institute *Global Status of CCS 2024*; 2024. https://www.globalccsinstitute.com/resources/global-status-report/

(52) Nordbotten, J. M.; Fernø, M. A.; Flemisch, B.; et al. Benchmarking CO_2 storage simulations: Results from the 11th Society of Petroleum Engineers Comparative Solution Project. *Int. J. Greenhouse Gas Control* **2025**, *148*, No. 104519.
(53) Shukla, R.; Ranjith, P.; Haque, A.; Choi, X. A Review of Studies on CO2 Sequestration and Caprock Integrity. *Fuel* **2010**, *89* (10), 2651−2664.
(54) Cui, G.; Hu, Z.; Wang, Y.; Jiang, S.; Wang, R. Migration Characteristics and Local Capillary Trapping Mechanism after the CO2 Leakage out of Saline Aquifers. *Fuel* **2024**, *356*, No. 129347.
(55) Ren, B. Local Capillary Trapping in Carbon Sequestration: Parametric Study and Implications for Leakage Assessment. *International Journal of Greenhouse Gas Control* **2018**, *78*, 135−147.

https://doi.org/10.1021/acs.est.5c08417
Environ. Sci. Technol. 2026, 60, 6149−6161